BaAu$_x$Zn$_{13-x}$: Electron-Poor Cubic NaZn$_{13}$-Type Intermetallic and Its Ordered Tetragonal Variant

Shalabh Gupta and John D. Corbett*

Ames Laboratory and Department of Chemistry, Iowa State University, Ames, Iowa 50011, United States

Ⓢ *Supporting Information*

ABSTRACT: Cubic NaZn$_{13}$-type (Fm-$3c$, Z = 8) BaAu$_x$Zn$_{13-x}$ compounds in the regions $1 \leq x \leq 5.4$ (a = 12.418(1)−12.590(1) Å) and $6.4 \leq x \leq 8$ (a = 12.630(1)− 12.660(1) Å) plus an ordered tetragonal variant near x = 6 ($P4/nbm$; a = 8.8945(4) Å, c = 12.646(1) Å; Z = 4) have been synthesized and characterized by means of X-ray diffraction. Although the cubic structure contains Zn-centered, mixed (Zn, Au) icosahedra connected in alternate orientations via mixed tetrahedral stars (TS), the icosahedron vertices are ordered in the tetragonal structure. Both the inner and the outer tetrahedra in the TS in the cubic phase consist of mixed Au and Zn atoms, whereas the tetragonal phase features three

different coloring schemes: inner Zn and outer Au tetrahedra, vice versa, or mixed Au and Zn sites on both inner and outer tetrahedra. Barium atoms center 24-atom snub cuboctahedra. Ordering of Au and Zn in the tetragonal phase achieves the largest number of heteroatomic Au−Zn contacts and yields relatively larger Hamilton populations (−ICOHPs) compared with homoatomic counterparts according to LMTO-based electronic structure calculations and analysis. Larger overlap populations are also observed for inter- versus intraicosahedral interactions. The densities-of-states data suggest the phase is metallic with highly dispersed Au d bands and nearly free-electron-like s and p bands for both Au and Zn.
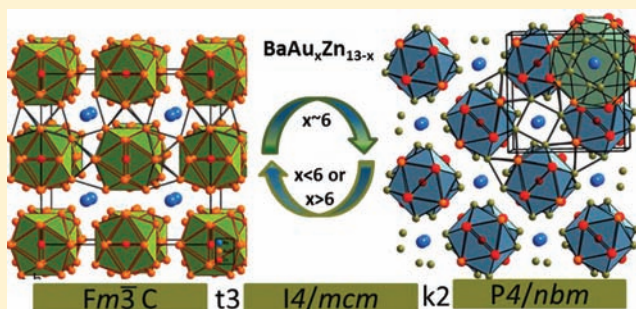
INTRODUCTION

Tuning valence electron concentrations (*vec*) in the electron-poor regions (i.e.,with average electron counts per atom (e/a) $\approx 1.5-2.5$) of some complex polar intermetallic systems has in recent years been rewarding, particularly in terms of the novel crystal structures that afford some understanding of the complex multicentered delocalized bonding often encountered.[1,2] Ternary polar intermetallic compounds are often formed between the electropositive metals from groups 1 and 2, relatively electronegative late transition metals, and main-group metals or metalloids.[3] Electron-precise Zintl phases are usually formed when the later members lie beyond group 13 (over the "Zintl border"), and these transition to more metal-like compounds with high coordination numbers on moving to triels (Ga, In, and Tl) and further to the left in the periodic table.[1,4] The last systems are usually too electron poor to achieve closed-shell configurations with only classical 2c−2e or cluster bonds, and this leads to optimization of the bonding in delocalized (multicentered) electronic states in structures with higher coordination numbers. Further reductions in *vec* by inclusion of late 4d and 5d elements such as Cd, Pt, Au, and Hg yield new structures and chemical insights into factors that govern the crystallographic and electronic structures.[5−8] Quantum mechanical calculations of electronic band structures at the density functional level and Hamilton population analyses (−ICOHP) have made it clear that the heteroatomic polar interactions between the d- and the p-block metals are

important to stability and that the large relativistic effects for the heavy late transition metals, gold particularly, enhance participation of 5d orbitals in both hetero- and homoatomic interactions.[7,9] Mixing of the contracted 6s and expanded 5d orbitals is also reflected in effectively reduced metallic radii and enhanced electronegativities compared with their lighter congeners.[10] Such notable effects have led us to investigate numerous ternary systems of gold and other later transition or early p elements such as Zn, Cd, In, and Tl. The present exploration of the Ba−Au−Zn system has led to the discovery of the cubic NaZn$_{13}$-type[11] BaAu$_x$Zn$_{13-x}$ ($1 \leq x \leq 8$) solutions and a new tetragonal variant at $x \approx 6$.

NaZn$_{13}$-type structures occur widely among binary and ternary systems[12] and have been investigated regarding bonding around the border between classical Zintl phases (e/a $\approx 3.5-4$) and "classical" intermetallic compounds (e/a ≤ 2). Nordell and Miller[13] concluded that the BaCu$_x$Al$_{13-x}$ version is stabilized within a narrow composition range that conforms to the *vec*-based arguments for optimum stability presented by Häussermann et al.[14] The latter asserted that structures built from tetrahedral star (TS) like motifs, as seen in the NaZn$_{13}$ archetype, are stable only within the *vec* range of 2.1−2.6. We report here the syntheses and crystal structures of the relatively electron-poorer BaAu$_x$Zn$_{13-x}$ compositions in the same

structure type over the (discontinuous) solution region $1.43 \leq e/a \leq 1.73$ that also contains a new tetragonal modification at $x \approx 6$.

■ EXPERIMENTAL SECTION

Syntheses. Syntheses started with dendritic Ba (Alfa-Aesar, 99.99%, surface scraped clean with scalpel), Au pieces (Ames laboratory, 99.995%), and Zn shot (Alfa-Aesar, 99.999%). Weighings were carried out in a nitrogen-filled glovebox with moisture levels ≤ 1 ppm, whereas all postreaction manipulations were carried out in air after it was established that the products are kinetically stable in air at room temperature for months. In a typical reaction, selected proportions of the elements (~400 mg total) were weld sealed in ~9 mm diameter Ta containers under Ar followed by their enclosure in an evacuated fused silica jacket to prevent oxidation of Ta by air at reaction temperatures. Syntheses were initiated at 700 °C for 12 h, quenched, annealed at 600 °C for 1 week, and quenched again. First evidence of a cubic $NaZn_{13}$-type structure came from a single crystal from the exploratory (nonstoichiometric) reaction of $BaAu_2Zn_5$. The structural parameters for this (IV) are given in the Supporting Information. Reactions over the composition range $1 \leq x \leq 9$ were then run because the structure and refined composition ($x = 5.20$) suggested possible continuous solid solutions $BaAu_xZn_{13-x}$ starting from isotypic $BaZn_{13}$.[12] A new tetragonal variant was also recognized for $x = 6$. For samples with $x > 7$, initial 800 °C reactions were employed as some unreacted gold remained at lower temperatures. These were then re-equilibrated at 600 °C as for the others. All products have a metallic luster. Estimated X-ray phase analyses and refined metrics of the cubic and tetragonal $BaAu_xZn_{13-x}$ are presented for all samples in Table 1. All syntheses across the x range were run in duplicate, and each pair gave substantially the same patterns, proving that the systems were in equilibrium.

Table 1. Refined Lattice Parameters (Angstroms) and Phase Analyses of the Cubic and Tetragonal $BaAu_xZn_{13-x}$ Phases from the X-ray Powder Diffraction Data

nominal comp.	lattice params[a]	phase analyses[b]
$BaAuZn_{12}$	12.4185(8)	>95% C
$BaAu_{2.00}Zn_{11}$	12.4485(9) (I)[c]	>95% C
$BaAu_2Zn_5$	12.4770(4) (IV)[d]	C (minor phase) + unidentified phase
$BaAu_3Zn_{10}$	12.5015(9)	~90% C, extra peaks at $2\theta = 31.56$, 32.90, and 33.76°
$BaAu_{3.50}Zn_{8.50}$	12.5126(8)	>95% cubic phase
$BaAu_{3.75}Zn_{9.25}$	12.5224(9)	~90% C; extra peaks at $2\theta = 23.56$ and 41.85°
$BaAu_{4.25}Zn_{8.75}$	12.539(1)	>95% cubic phase
$BaAu_{4.75}Zn_{8.25}$	12.5575(8)	~90% C; extra peaks at $2\theta = 31.31$ and 32.65°
$BaAu_{5.00}Zn_{8.00}$	12.5652(7)	~90% C
$BaAu_{5.20}Zn_{7.80}$	12.587(1)	~90% C; extra peaks at $2\theta = 23.52$, 48.91, and 58.56°
$BaAu_{5.40}Zn_{7.60}$	12.5898(7)	~90% C; extra peaks at $2\theta = 23.52$, 31.35, and 43.62°
$BaAu_{5.80}Zn_{7.20}$	$a = 8.8998(2)$, $c = 12.625$ (I)[d]	90% T[b]
$BaAu_{6.00}Zn_{7.00}$	$a = 8.8945(4)$, $c = 12.646(1)$ (III)[c]	95% T
$BaAu_{6.20}Zn_{6.80}$	$a = 8.9000(3)$, $c = 12.6469(8)$	90% T
$BaAu_{6.40}Zn_{6.60}$	12.631(1)	95% C
$BaAu_{6.50}Zn_{6.50}$	12.635(1)	95% C
$BaAu_{7.00}Zn_{6.00}$	12.641(2) (II)[c]	95% C
$BaAu_{8.00}Zn_{5.00}$	12.660(1)	95% C

[a]As quenched from 600 °C. [b]C, = cubic; T = tetragonal. [c]Single crystal data in text. [d]Single crystal data in the Supporting Information.

Powder X-ray Diffraction. Phase analysis by X-ray powder diffraction experiments was carried out on well-ground samples that were homogeneously spread on Mylar film with the aid of a thin layer of Apiezon vacuum grease. Data were recorded at room temperature on a Huber 670 Guinier camera equipped with an image plate detector and Cu Kα radiation (λ = 1.540598 Å). The diffractometer was calibrated with NBS Si 640b standard, and a detection limit for the second phase was conservatively estimated to be ~5 vol. % in equivalent scattering power. Data were recorded in the 2θ range of 4–100° with step sizes of 0.005° and exposure times of 30 min. Unit cell parameters were obtained by least-squares refinements on 15–20 peaks in the 2θ range of 10–100° with the aid of the WinXPow program[15] and were subsequently employed in all distance calculations from single-crystal positional refinements. Yields and phase distributions for all reactions (Table 1) were estimated from detailed comparisons of patterns of synthetic products with those calculated[15] for the refined structures reported here or elsewhere. Lattice dimensions are also very useful in the differentiation of compositions (below).

Single-Crystal Structure Determination. *Cubic $BaAu_{2.02(4)}Zn_{10.98}$ (I) and $BaAu_{6.61(1)}Zn_{6.31}$ (II).* Cubic crystal structures of samples from both the gold-poor ($x < 6$) and -richer ($x \geq 7$) regions were refined by single-crystal X-ray

Table 2. Crystal, Data Collection, and Refinement Parameters for the Cubic and Tetragonal $BaAu_xZn_{13-x}$

loaded comp.	$BaAu_2Zn_{11}$(I)	$BaAu_7Zn_6$ (II)	$BaAu_6Zn_7$ (III)
emp. formula	$BaAu_{2.02(4)}Zn_{10.98}$	$BaAu_{6.61(1)}Zn_{6.31}$	$BaAu_{5.93(2)}Zn_{7.07}$
cryst syst	cubic	cubic	tetragonal
space group, Z	$Fm\text{-}3c$ (226), 8	$Fm\text{-}3c$, 8	$P4/nbm$ (125), 4
unit cell dimens/Å	12.4485(7)	12.641(2)	8.8945(4), 12.646(1)
vol./Å^3	1929.1(2)	2019.8(4)	1000.4(1)
ρ_{calcd}/g·cm^{-3}	8.610	12.443	11.796
μ/mm^{-1}	61.007	117.428	107.82
reflns collected	3457	3604	10 744
independent obsd reflns; R_{int}	123, 0.0362	125, 0.0776	685, 0.0867
data/params	123/11	125/12	685/47
GoF on F^2	1.186	1.171	1.109
R1, wR2 [I > 2σ(I)]	0.0139, 0.0273	0.0181, 0.0340	0.0315, 0.0512
R1, wR2 (all data)	0.0164, 0.0280	0.0212, 0.0345	0.0553, 0.0571
$\Delta\rho_{max}$, $\Delta\rho_{min}$/e Å^{-3}	0.809, −0.536	1.051, −0.897	1.766, −1.526

diffraction means, Table 2. Well-faceted but irregularly shaped crystals were picked from powdered samples under an optical microscope and secured on the tip of a capillary with Apiezon grease. Intensity data were collected at 293(2) K on a Bruker Smart Apex diffractometer equipped with Mo Kα radiation (λ = 0.71073 Å). A total of 1800 frames, 10 s each, were collected up to $2\theta = 56.48°$. The intensities were integrated with the SAINT program[16] in the SMART software package for the indicated F-centered cubic cell and corrected for Lorentz, polarization, and absorption effects, the last empirically with the aid of SADABS.[17] Merging of these with the XPREP program in the SHELXTL v 6.1[18] program package yielded 123 independent reflections for structure I ($R_{int} = 3.62\%$) and observed [I > 2σ(I)]. Systematic absence analysis indicated space group $F\text{-}43c$ or $Fm\text{-}3c$, and the latter centrosymmetric one was chosen on the basis of $\langle E^2 - 1 \rangle$ statistics. The initial model indicated by direct methods was refined by full-matrix least-squares method on F^2 for three sites tentatively assigned as

Table 3. Coordinates and Isotropic-Equivalent Thermal Displacement Parameters (Å^2) for Cubic $BaAu_{2.02(4)}Zn_{10.98}$ (I) and $BaAu_{6.61(1)}Zn_{6.31(1)}$ (II), Respectively

	Wyck	sym	x	y	z	site occupancy	U_{eq}
Au1/Zn1	96i	1	0	0.1797(1)	0.1188(1)	0.233(2)/0.767	7(1)
			0	0.1795(1)	0.1221(1)	0.551(5)/0.449	18(1)
Zn2	8b	..m	0	0	0	1	6(1)
			0	0	0	0.924(6)	24(1)
Ba	8a	..m	1/4	1/4	1/4	1	5(1)
			1/4	1/4	1/4	1	10(1)

Table 4. Coordinates and Isotropic-Equivalent Displacement Parameters for Tetragonal $BaAu_{5.80(2)}Zn_{7.20}$ (III)

	Wyck	sym	x	y	z	site occupancy	U_{eq}
(Au/Zn)1	16n	1	0.1898(1)	0.0535(1)	0.2526(1)	0.502(6)/0.498	17(1)
(Au/Zn)2	8m	..m	0.3718(1)	0.6283(1)	0.4278(1)	0.914(3)/0.086	19(1)
(Au/Zn)3	8m	..m	0.3718(1)	0.6282(1)	0.0702(1)	0.129(2)/0.871	17(1)
(Au/Zn)4	8m	..m	0.5751(1)	0.4300(1)	0.1275(1)	0.792(4)/0.208	18(1)
(Au/Zn)5	8m	..m	0.5700(1)	0.4250(1)	0.3705(1)	0.127(3)/0.873	16(1)
Zn6	4h	2.mm	3/4	1/4	0.2497(2)	1	21(1)
Ba1	2b	422	1/4	1/4	1/2	1	11(1)
Ba2	2a	422	1/4	1/4	0	1	11(1)

Au1 (96i), Ba1 (8a), and Zn2 (8b), respectively. Judging from the isotropic displacement parameters, the assigned Au1 site was eventually refined as fully occupied by a mixture of Au1 (23.3(2)%) plus Zn1 and the 8a and 8b positions as fully occupied. With the hindsight gained from later refinement of the 8b Zn2 in the Au-richer phase II, this site occupancy was re-refined to ~98.2(2)% of the total and then reset to full occupancy during final refinements. The refinement process for I concluded with anisotropic refinement of thermal parameters to gain R1, wR2, and GoF values of 1.39%, 2.73%, and 1.186, respectively. The largest residual peak and hole in the ΔF map were insignificant, 0.809 and −0.536 e·Å^{-3}, which are 0.6 Å from Au1/Zn1. However, X-ray pure samples for some cubic phases within the region $3 \leq x < 6$ did not yield any suitable single crystals.

Single crystals of II were obtained from the reaction composition $BaAu_7Zn_6$ (x = 7). All data collection and refinement strategies paralleled those for I. The occupancy of the 8b Zn site was noteworthy as its initial U_{iso} value was comparatively high (28(1) vs 18(1) and 10(1) Å^2 for 96i and 8a positions, respectively). Occupancy refinement of Zn gave 0.924(6) and smaller displacement parameters. Fractional Zn occupancies for the 8b sites in other $NaZn_{13}$-type structures have been reported for $EuZn_{13-x}$ (74.8(7) %) and in $AeZn_{13-\delta}$ systems with occupancies of 74(1)%, 78(1)%, and 89(1)% for Ae = Ca, Sr, and Ba, respectively; the first two reactions contained excess Zn, and the others were loaded on stoichiometry.[19,20] Since the composition of $BaAu_{6.61(1)}Zn_{6.31(1)}$ (II) is close to that of the tetragonal phase (below), data were also collected for the same crystal at 173 K to ensure the absence of a low-temperature transition.

Tetragonal $BaAu_{5.93(2)}Zn_{7.07}$ (III). Single crystals from two $BaAu_6Zn_7$ reactions gave refined compositions of $BaAu_{5.93(2)}Zn_{7.07}$ (III) and $BaAu_{5.80(3)}Zn_{7.20}$ (V, Table S1, Supporting Information) within 4σ of each other. Lattice constants were measured for two other crystals from each product, and they likewise differed by 3−4σ, indicating that samples were reasonably homogeneous. Several irregular crystals of III were separated from the coarsely ground powder. A total of 2400 frames collected from one crystal with 10 s frame exposures yielded 10 744 reflection out of which 685 were independent (R_{int} = 0.0867). According to the systematic absence conditions and statistical tests, the centrosymmetric space group $P4/nbm$ (No. 125) was chosen. Direct methods yielded an initial model with nine atomic positions, one of which was discarded because of unphysical distances to other atoms. A few cycles of refinement resulted in residual values below 10%, indicating the correctness of the chosen space group. Initially six of eight atoms were tentatively assigned as gold and two as barium

judging by distances to their nearest neighbors (Ba > 3.6 Å; Au ≈ 2.6−2.9 Å). Further refinement resulted in either too large or too small comparative displacement parameters for all Au positions, and five of six were subsequently refined as mixed Au/Zn and one as fully occupied Zn (within 3σ). Final anisotropic refinements resulted in well-behaved displacement ellipsoids with a nearly featureless ΔF map. Structure refinement of V proceeded similarly, Table S2, Supporting Information. Atomic coordinates, standardized with *STRUCTURE TIDY*[21] (as implemented in the WinGX software package[22]) for crystals I−III are given in Tables 3 and 4. Anisotropic displacement parameters for all data sets and interatomic distances for II, III, and V are available in Supporting Information Tables S4 and S5.

Electronic Structure Calculations. The tight-binding linear muffin-tin-orbital (TB-LMTO) method employing the atomic sphere approximation (ASA)[23,24] as implemented in the Stuttgart code was used for self-consistent electronic structure calculations.[25] An ordered model of the tetragonal phase was built in the lower symmetry space group $Pban$ (No. 50). Exclusion of the 4-fold axis breaks the degeneracy of the 16n sites that are co-occupied by Au and Zn in about a 1:1 ratio. The two positions so generated were "colored" as Au and Zn, whereas the rest were treated as pure Au or Zn. The radii of the Wigner−Seitz spheres were assigned automatically, subjected to a 16% overlap restriction between atom-centered spheres.[26] This filled the unit cell with a 7.82% volume overlap without the need to introduce any empty spheres. Exchange and correlation were treated by the local density approximation (LDA), which was parametrized according to von Barth and Hedin.[27] Relativistic effects were taken into account using a scalar approximation.[28] A basis set of Ba 6s/6p/5d, Zn 3s/3p, and Au 6s/6p/5d/5f (Ba 6p and Au 5f downfolded[29]) was employed, and the reciprocal space integrations were performed on grids of 138 irreducible k points. For bonding analysis, the energy contributions of all filled electronic states for selected atom pairs were calculated by the COHP (crystal orbital Hamilton population) method, and these were also integrated up to E_F to give −ICOHP values.[30]

■ RESULTS AND DISCUSSION

Syntheses and Phase Analyses. High yields (>90%) of cubic $BaAu_xZn_{13-x}$ were obtained for the nominal compositions $1 \leq x \leq 3.75$, $4.25 \leq x \leq 5.40$, and $6.40 \leq x \leq 8$. (There is some deviation at x = 8, Figure 1, perhaps because of nonstoichiometry.) The other lattice parameters increase linearly with x as shown in Figure 1, consistent with the larger 12-coordinate radius of elemental Au (1.439 Å) compared with
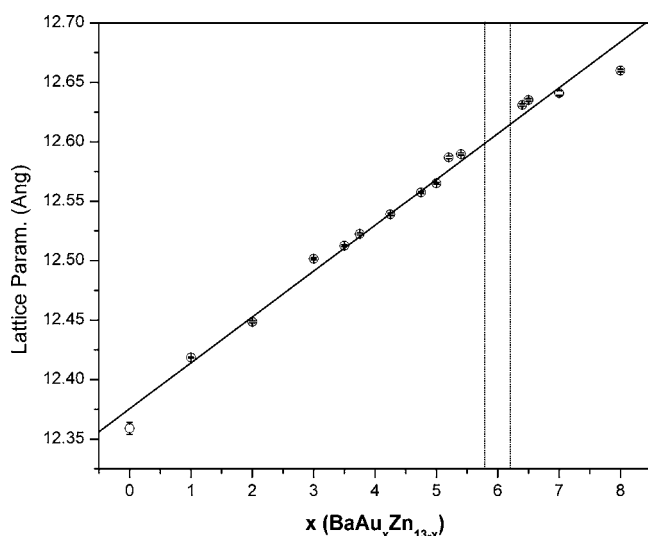
Figure 1. Variation of the lattice parameter with x in cubic $BaAu_xZn_{13-x}$. Tetragonal phase region occurs between the two dotted lines. Open circle at $x = 0$ is the literature parameter for $BaZn_{13}$.[31]

that of Zn (1.379 Å).[32] Surprisingly, the reactions for $x = 3.85$, 4.0, and 4.15 yielded only modest amounts of a regular cubic phase, but these did not grow to useful sizes for single-crystal diffraction. Some new overgrowth may be responsible. (Powder pattern examples in this region are shown in Supporting Information Figure S1.) One or more additional phase(s) formed that were also available only as microcrystals and could not be identified solely from their power pattern(s) in terms of any known binary or ternary phase in this system. They occurred reproducibly across multiple loadings and interfered with lattice constant calculations for the cubic component in this region. Similar reactions after quenching the starting mixture from 700 °C and annealing at 600 °C for 7 days and 450 °C for 10 days did not change the product profile. The extra diffraction pattern from these samples was not that of the reported I-centered $NaZn_{13}$-type structure ($tI56$, space group $I4/mcm$).[33] However, ~90−95% yields of cubic phases were obtained for the neighboring $x = 3.75$ and 4.25.

The tetragonal phase is obtained for $5.6 \leq x \leq 6.20$, and the cubic structure is again stable between $x \approx 6.40$ and 8.0. The composition $BaAu_9Zn_4$ ($x = 9$) yielded broad diffraction peaks, and the samples could not be well pulverized, but a cubic phase or elemental gold were not detected in the powder pattern. A $BaAu_{13}$ composition, from arc melting the elements followed by annealing at 800 °C for 1 week, yielded $BaAu_5$[34] ($CaCu_5$-type, $P6/mmm$) along with the unreacted Au.

The composition $BaAu_6Zn_7$ ($x = 6$) yielded the pure tetragonal variant, and two single crystals (including III) yielded lattice parameters within 3σ of each other and refined compositions within 4σ, indicating that the sample was probably well homogenized. Another crystal from a different reaction with the same loaded composition yielded $BaAu_{5.80(3)}Zn_{7.20}$ (V, Supporting Information), differing by less than 4σ from the earlier composition. Reactions with $x = 5.80$ and 6.20 also yielded ~90% tetragonal phase. Although the powder patterns of the cubic and the tetragonal phases are grossly similar, the strong 212 reflection can only be indexed for the latter.

Structures. *Cubic $BaAu_xZn_{13-x}$.* A near [001] projection of the face-centered lattice ($NaZn_{13}$ type) is shown in Figure

2a. The three crystallographic sites $8a$, $8b$, and $96i$ are occupied by Ba (aqua), Zn (red), and mixed Au/Zn (orange),
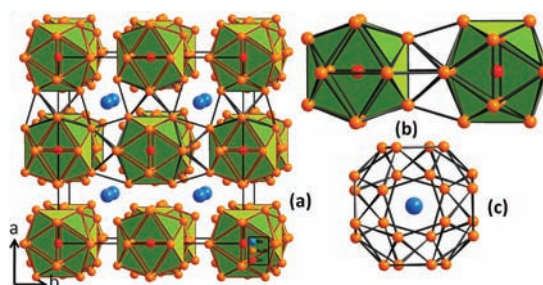
Figure 2. (a) Approximate (001) projection of the cubic $BaAu_xZn_{13-x}$ showing the packing of Zn-centered (red) icosahedra with uniform Au/Zn mixed vertices (orange). (b) Tetrahedral stars connecting the icosahedra. (c) Twenty-four-atom snub cubes centered by Ba (aqua).

respectively. The first two form a cubic CsCl-type lattice, eight such cubes define the unit cell, and the $96i$ ($Zn_{12-x}Au_x$) atoms form near-icosahedra that are centered by Zn. These icosahedra are linked to one another in an alternating (90°) orientation (Figure 2b) via $\{(Au,Zn)_4(Au,Zn)_4\}$ tetrahedral stars, as highlighted in Figure 2a and 2b. This arrangement generates 24-atom snub cubes around Ba that have six square faces and 32 triangles (Figure 2c). The snub cubes share all square faces with other cubes (Figure S2, Supporting Information) and eight of 32 triangular faces with the surrounding icosahedra. Since the vertices of the icosahedra ($96i$) also define the tetrahedral stars, the latter can be used alone to describe the complete crystal structure, as Haüssermann et al.[14] used to present a rational basis for the 'stability' of this structure type according to the Zintl−Klemm electron-counting rules. The occupancies of the $96i$ position range from ~8% gold (1 Au per 12 icosahedral vertices) in $BaAuZn_{12}$ to ~66% (8Au + 4Zn per icosahedron) in $BaAu_8Zn_6$, Table 1. These are estimated only from the single-phase powder patterns of the loaded $BaAu_xZn_{13-x}$ compositions, i.e., those that melt congruently.

As also noted earlier for isostructural $BaCu_xAl_{13-x}$, the icosahedra in the cubic $BaAu_xZn_{13-x}$ are not perfect (point symmetry T_h) rather the edges ($96i$−$96i$) differ by ~5−6%.[13] Subtle changes at the $96i$ site follow changes in gold proportions. For $BaAu_{6.61(1)}Zn_{6.31}$ up to ~8% differences in the edge lengths suggest that greater distortions are induced by larger gold proportions. Another notable difference is ~8% Zn ($8b$) deficiency in the gold-richer phase (II). It has been argued that such vacancies may occur for electronic reasons as they have only been observed in the electron-richer binary $AeZn_{13-\delta}$ (Ae = Ca, Sr, Ba) and not for AZn_{13} (A = Na, K, Rb).[20] However, our results present limited evidence inasmuch as significant Zn vacancies are observed only in the gold-richer and nominally electron-poorer compositions rather than the zinc-richer examples. It is noteworthy that alternate mixed occupancies at the icosahedral centers ($8b$ sites) have been reported in the $BaCu_5Al_8$, $EuCu_{6.5}Al_{6.5}$, and $Sr_{0.5}Ba_{0.5}Ag_6Al_7$ structures.[13] The influence of the tetrahedra stars in structural stability emphasized in the earlier work[14] is clear from the relatively smaller intericosahedral distances (and larger −ICOHP values discussed later) as compared with the intraicosahedral distances here, Table S5, Supporting Information. Bond lengths in the gold-richer phases in general scale with the lattice parameter.
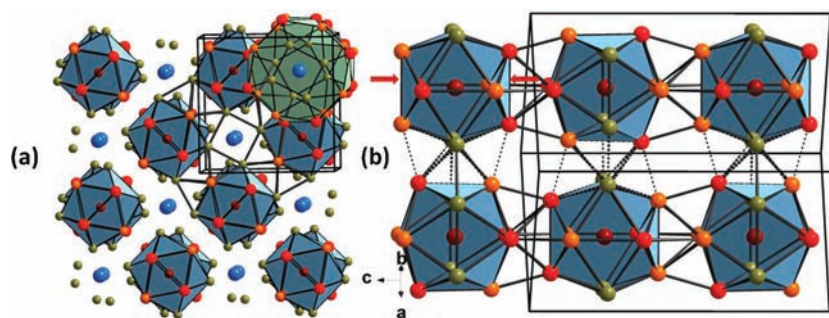
Figure 3. (a) Approximate (001) section of the tetragonal $BaAu_xZn_{13-x}$ ($x \approx 6$) showing packing of the nearly ordered Au (orange, $8m$) and Zn (red, $8m$) atoms and ~1:1 mixture of Au and Zn atoms (olive, $16n$) icosahedra centered by Zn (dark red, $4h$) and 24-coordinate snub cube centered by Ba (aqua). (b) Two different tetrahedral stars connect icosahedra in the ab plane and along c directions.

Tetragonal Phase. A near [001] projection of the structure of $BaAu_{5.93(2)}Zn_{7.07}$ is shown in Figure 3. The structure has a motif similar to that of the cubic phase, Zn-centered icosahedra with Au and Zn vertices that are connected in alternate orientations via tetrahedral stars, plus the Ba-centered Zn and Au snub cubes. However, the two structures are clearly different in the way the icosahedra are packed. The mixed $96i$ positions that define the icosahedral vertices and the tetrahedral stars in the cubic structure ($Z = 8$) are now split into one $16n$ and four $8m$ sites ($Z = 4$, Figure S3, Supporting Information). Although the unique $16n$ sites are co-occupied by Au and Zn in a ~1:1 ratio, two of the four 8-fold sites are preferentially occupied by Au and the other two by Zn, the minor components being 15% or less. The icosahedra in the tetragonal structure are thus constituted from five different ordered Au and Zn sites, such that the arrangement of atoms allows for the maximum number of heteropolar Au−Zn contacts. Since an icosahedron is constituted of triangles, decorating two types of atoms on the three corners of a triangle is akin to the arranging electronic spins on a triangular lattice and causing geometric magnetic frustration.[35] Elegantly, nature avoids such a scenario for 16 out of 20 triangles by co-occupation of one vertex type ($16n$) by Au and Zn in the ratio of ~1:1, depicted in olive in Figure 3. This leaves only two homoatomic contacts and these with the largest 3.063 Å separation per icosahedron, as marked by red arrows in Figure 3b. One might argue that two positions ($8m$) forming the homoatomic Zn−Zn and Au−Au contacts could mix statistically (without changing the composition) but that mixing would entail loss of two short (2.588 and 2.653 Å) and substantial heteroatomic, intericosahedral interactions (Table S5, Supporting Information).

The ordering of atoms in this symmetry per se helps to understand why this structure is adopted over a very narrow range of composition. Retention of the structure very far from $x \approx 6$ would require preferential occupation of the $16n$ sites by either Zn or Au, leading to more homoatomic ($16n-16n$) contacts of 3.0 Å or less. Further reduction of symmetry of course would overcome this constraint. It is not clear however why five of six anion sites are partially disordered. As shown in Figure 3b, two kinds of tetrahedral stars connect icosahedra, one along c and the other in the ab plane (solid and broken lines, respectively). Although both inner and the outer tetrahedra in the latter consist of two $16n$ vertices, one Zn and one Au, those along the c direction are composed of all inner gold and outer zinc tetrahedra or vice versa. Although the average inter- and intraicosahedral distances in the tetragonal $BaAu_{5.93(2)}Zn_{7.07}$ and the cubic $BaAu_{6.61(1)}Zn_{6.31(1)}$ compounds differ by <1%, the tetrahedral units in the former display some

distances <2.6 Å. Clearly, the shortest contacts with the largest −ICOHP values are observed between Au and Zn that form the outer edges (vertex to face capping) of the tetrahedral stars (2.588−2.658 Å). These distances also constitute the square faces of the snub cubes.

Although several ternary rare-earth-metal aluminides (RT_7Al_6) and silicides RT_7Si_6 are known with $NaZn_{13}$-type structures and mixed T/Al or T/Si sites, superstructure ordering near these compositions has been observed in only a few systems. For example, an I-centered tetragonal variant occurs for $Ce_2Ni_{17}Si_9$ ($CeNi_{8.5}Si_{4.5}$) ($tI56$, $I4/mcm$)[36] and an orthorhombic distortion for $LaNi_7In_6$ ($oI56$, $Ibam$).[37] Both feature icosahedra packed in a similar manner as in $NaZn_{13}$. Both the primitive tetragonal $BaAu_6Zn_7$ reported here and the I-centered cubic cell of $Ce_2Ni_{17}Si_9$ are derived from the cubic $NaZn_{13}$-type structure through the metric relationship $a_t \approx 1/2a_c - 1/2b_c$, $b_t \approx 1/2a_c + 1/2b_c$, and $c_t \approx c_c$. Not surprisingly, these structure types are related through a group−subgroup relation according to the Bärnighausen formalism[38] (Figure S3, Supporting Information). The space group symmetry is lowered from $F4/m-32/c$ (No. 226) for $NaZn_{13}$ to $I4/m2/c2/m$ (No. 140) for $CeNi_{8.5}Si_{4.5}$ by a *translationengleiche* reduction of index 3 (t3). This symmetry reduction splits the $96i$ positions that form the icosahedral vertices in the cubic structure into three 16-fold positions ($Z = 4$) in $CeNi_{8.5}Si_{4.5}$ with ordered Ni and Si. A *klassengleiche* symmetry reduction of index 2 further splits the two 16-fold positions into two 8-fold positions each in the primitive tetragonal $BaAu_6Zn_7$ structure ($P4/n2/b2/m$, No. 125) that are ordered by Au and Zn. It is clear that such symmetry reduction in tetragonal $BaAu_6Zn_7$ maximizes the favorable heteroatomic and reduces the unfavorable homoatomic interactions. Although the reasons for a second discontinuity here around $x = 4$ are still unclear, it seems plausible that another ordered structure forms at this composition but that its crystal growth is limited.

Electronic Structure and Bonding Analysis. The nearly fully ordered tetragonal $BaAu_{5.93(2)}Zn_{7.07}$ provides a good opportunity to study the electronic structure and analyze the pairwise bond populations, which may reveal reasons for the atomic ordering around this composition. Calculations were carried out on an ordered ($Pban$) version of the structure in which the degeneracies of the mixed $16n$ positions are broken. (The resulting 'coloring' of these sites is shown in Figure S2, Supporting Information.) Densities-of-states (DOS) and crystal Hamilton overlap population (−COHP) data appear in Figure 4. Significant densities-of-states at the Fermi level and below a pseudogap at ~2 eV indicate the compound is metallic and electron poor. Major contributions to the DOS at E_F come
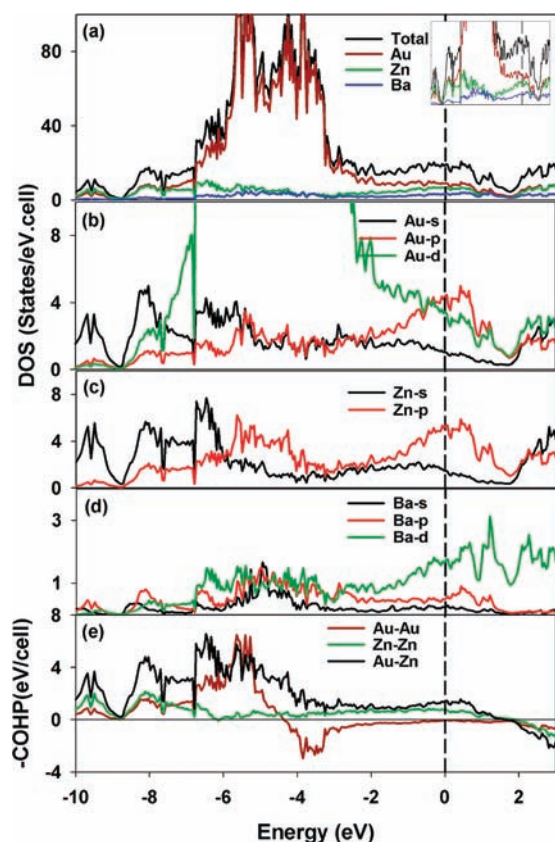
Figure 4. Total-, atom-, and orbital-projected DOS data (a–d) and −COHP results (e) for the ordered tetragonal $BaAu_6Zn_7$ in *Pban* space group. Zn d orbitals are treated as a pseudo core.

from the Zn 4p and Au 6p bands. The Au 5d are split into a narrow band at ∼−8 eV and a highly dispersed band spanning from −7 to 2 eV. The bottom of the valence band at ∼−10.5 eV is defined mainly by the Zn s orbitals, and the Zn 3d band is fairly localized below −7 eV. A distinct drop in DOS is observed at ∼1.6 eV, which corresponds to ca. 5.5 e^-/fu. As estimated from the integrated values of DOS at the Fermi energy (IDOS), s and p orbitals on Zn and Au together contribute ∼30% of the states, the rest being the 3d and 5d. The significant number of filled p states from both Au and Zn is in line with their substantial reduction in this phase. Barium makes only ca. 3% contribution to the IDOS. Hamilton overlap populations were calculated in order to analyze the atomic interactions within the structure. Values of −ICOHP per bond (Table S3, Supporting Information) are clearly segregated into three distinct regions of the structure, Figure 5. The smallest values correspond to the interactions between Zn at icosahedral centers (4*h*) and the Au and Zn vertices (0.216−0.326 eV), whereas the largest values (average 1.1 eV) are for intericosahedral interactions (essentially the tetrahedral stars). Intermediate values averaging 0.7 eV are noted for the intraicosahedral contacts. Overall, the overlap populations are greater for Au−Zn and Au−Au pairs compared with Zn−Zn. As evidenced from the −COHP plots, Au−Au interactions are nonbonding whereas Au−Zn and Zn−Zn interactions are not optimized at E_F, leaving a few unfilled bonding states there above. Of course, these calculations do not address thermodynamic questions about the stability of this phase. Similar considerations of the bonding in the cubic $BaAu_xZn_{13−x}$ would be very difficult because of the large reduction in
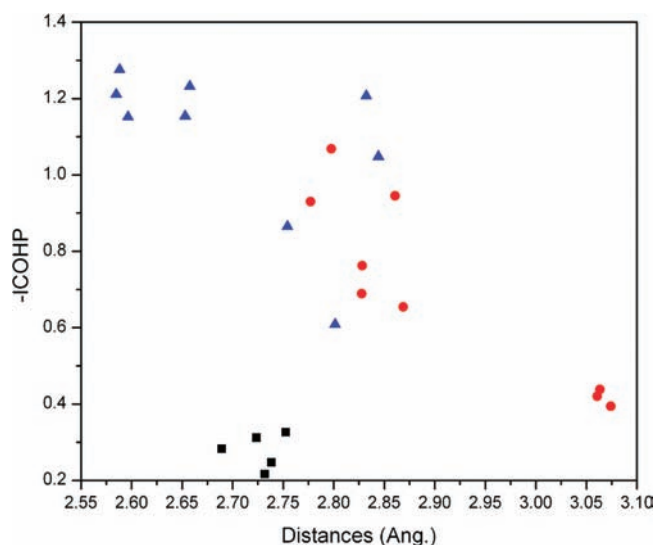
Figure 5. Distances (Angstroms) vs −ICOHP/bond in the ordered tetragonal $BaAu_6Zn_7$. Interactions between the central Zn and the icosahedral vertices (black), intraicosahedral (red), and intericosahedral interactions (blue) are marked.

symmetry necessary to gain a model with only pure elements on the lattice sites.

■ CONCLUSIONS

These studies on the ternary $BaAu_xZn_{13−x}$ system appear to be the first comprehensive investigation of a complete solid solution range in any $NaZn_{13}$-type ternary system. These reveal the large range of stoichiometries possible plus a new and closely related tetragonal intermediate with a narrow composition range. The new examples presented here are among the electron-poorest compounds with a $NaZn_{13}$-type structure, e/a ≈ 1.5 − 2.1, excluding Au d^{10}. These shed light on the importance of crystal packing and bond polarities in intermetallic structures that are often understood only in terms of their optimized electronic structures. The tetragonal phase is structurally closely related to the $NaZn_{13}$ structure and features Zn-centered icosahedra with Au and Zn vertices. Electronic structure calculations on this clearly reveal greater overlap populations among the intericosahedral interactions. The −ICOHP data suggest heteroatomic contacts (larger bond populations) are of paramount importance at this particular composition. The reappearance of the cubic phase at higher *x* with randomly distributed Au and Zn atoms suggests a delicate interplay between enthalpy- and entropy-driven terms. These results provoke rethinking of closed-shell electronic requirements for the basic cluster units, and recognition that other factors such as packing should be included.

■ ASSOCIATED CONTENT

ⓢ Supporting Information
Observed powder patterns for *x* = 3.8 and 4.0 that lack macrocrystal growth and that calculated for a nearby $BaAu_{2.02}Zn_{10.98}$; crystallographic information for cubic $BaAu_2Zn_5$ (IV) and $BaAu_6Zn_7$ (V); anisotropic displacement parameters for all structures reported; interatomic distances in cubic I and II and tetragonal III; −ICOHP data for tetragonal $BaAu_6Zn_7$; group−subgroup relationships among cubic $BaAu_xZn_{13−x}$ (*Fm-3c*), body-centered (*I4/mcm*) and primitive tetragonal derivatives (*P4/nmb*) versions; illustrations of snub

cubes in cubic and tetragonal phases; views of ordered $BaAu_6Zn_7$ in *Pbam*. This material is available free of charge via the Internet at http://pubs.acs.org.

■ AUTHOR INFORMATION

Corresponding Author
*E-mail: jcorbett@iastate.edu.

■ ACKNOWLEDGMENTS

■ REFERENCES

(1) Corbett, J. D. *Inorg. Chem.* **2010**, *49*, 13.
(2) Lin, Q.; Corbett, J. D. *Struct. Bonding (Berlin)* **2009**, *133*, 1.
(3) In *Chemistry, Structure and Bonding of Zintl Phases and Ions*; Kauzlarich, S., Ed.; VCH Publishers: New York, 1996; Chapter 3.
(4) Corbett, J. D. *Angew. Chem., Int. Ed.* **2000**, *39*, 670.
(5) Samal, S. L.; Corbett, J. D. *Inorg. Chem.* **2011**, *50*, 7033.
(6) Palasyuk, A.; Corbett, J. D. *Z. Anorg. Allg. Chem.* **2007**, *633*, 2563.
(7) Li, B.; Kim, S.-J.; Miller, G. J.; Corbett, J. D. *Inorg. Chem.* **2009**, *48*, 6573.
(8) Dai, J.-C.; Gupta, S.; Gourdon, O.; Kim, H.-J.; Corbett, J. D. *J. Am. Chem. Soc.* **2009**, *131*, 8677.
(9) Wang, F.; Pearson, K. N.; Straszheim, W. E.; Miller, G. J. *Chem. Mater.* **2010**, *22*, 1798.
(10) Pyykkö, P. *Chem. Rev.* **1988**, *88*, 563.
(11) Shoemaker, D. P.; Marsh, R. E.; Ewing, F. J.; Pauling, L. *Acta Crystallogr.* **1952**, *5*, 637.
(12) Villars, P.; Calvert, L. D. *Pearson's Handbook of Crystallographic Data for Intermetallic Phases*, 2nd ed.; ASM International: Metals Park, OH, 1991.
(13) Nordell, K. J.; Miller, G. J. *Inorg. Chem.* **1999**, *38*, 579.
(14) Häussermann, U.; Svensson, C.; Lidin, S. *J. Am. Chem. Soc.* **1998**, *120*, 3867.
(15) *WinXPow 2.10*; Stoe & Cie GmbH: Darmstadt, Germany, 2004.
(16) *SAINT*; Bruker AXS, Inc.: Madison, WI, 2000.
(17) Blessing, R. H. *Acta Crystallogr. A* **1995**, *51*, 33.
(18) *SHELXTL 6.14*; Bruker AXS, Inc.: Madison, WI, 2000.
(19) Saparov, B.; Bobev, S. *J. Alloys Compd.* **2008**, *463*, 119.
(20) Wendorff, M.; Röhr, C. *J. Alloys Compd.* **2006**, *421*, 24.
(21) Gelato, L. M.; Parthé, E. *J. Appl. Crystallogr.* **1987**, *20*, 139.
(22) Farrugia, L. J. *J. Appl. Crystallogr.* **1999**, *32*, 837.
(23) Andersen, O. K.; Jepsen, O. *Phys. Rev. Lett.* **1984**, *53*, 2571.
(24) Andersen, O. K. *Phys. Rev.* **1975**, *B12*, 3060.
(25) Krier, G.; Jepsen, O.; Burkhardt, A.; Andersen, O. K. *TB-LMTO-ASA Program*, v4.7; Max-Planck Institut für Festkörperforschung: Stuttgart, Germany, 1995.
(26) Jepsen, O.; Andersen, O. K. *Z. Phys. B* **1995**, *97*, 35.
(27) von Barth, U.; Hedin, L. *J. Phys. C: Solid State Phys* **1972**, *5*, 1629.
(28) Koelling, D. D.; Harmon, B. N. *J. Phys. C: Solid State Phys* **1977**, *10*, 3107.
(29) Löwdin, P. *J. Chem. Phys.* **1951**, *19*, 1396.
(30) Dronskowski, R.; Blöchl, P. *J. Phys. Chem.* **1993**, *97*, 8617.
(31) Bruzzone, G.; Ferretti, M.; Merlo, F. *J. Less-Common Met.* **1985**, *114*, 305.
(32) Pauling, L. *The Nature of the Chemical Bond*, 3rd ed.; Cornell University Press: Ithaca, NY, 1960; p 403.
(33) Bodak, O. I. *Kristallografiya* **1979**, *24*, 1280.
(34) Palenzona, A.; Bonino, G. B. *Atti Accad. Naz. Lincei, Cl. Sci. Fis., Mat. Nat., Rend.* **1967**, *42*, 504.
(35) Ramirez, A. P. In *Handbook of Magnetic Materials*; Buschow, K. J. H., Ed.; Elsevier Science: Amsterdam, 2001; Vol. 13, pp 423−520.
(36) Bodak, O. I. *Kristallografiya* **1979**, *24*, 732.
(37) Kalychak, Y. M.; Zaremba, V. I.; Galadzhun, Y. V.; Miliyanchuk, K. Y.; Hoffmann, R. D.; Pöttgen, R. *Chem.—Eur. J.* **2001**, *7*, 5343.
(38) Bärnighausen, H. *Commun. Math. Chem.* **1980**, *9*, 139.